J. Fluid Mech. (1991), *vol.* 224, *pp.* 241–260
Printed in Great Britain

Energy growth of three-dimensional disturbances in plane Poiseuille flow

By L. HÅKAN GUSTAVSSON

Division of Fluid Mechanics, Department of Mechanical Engineering, Luleå University of Technology, S-95187 Luleå, Sweden

(Received 9 January 1990 and in revised form 17 August 1990)

The development of a small three-dimensional disturbance in plane Poiseuille flow is considered. Its kinetic energy is expressed in terms of the velocity and vorticity components normal to the wall. The normal vorticity develops according to the mechanism of vortex stretching and is described by an inhomogeneous equation, where the spanwise variation of the normal velocity acts as forcing. To study specifically the effect of the forcing, the initial normal vorticity is set to zero and the energy density in the wavenumber plane, induced by the normal velocity, is determined. In particular, the response from individual (and damped) Orr–Sommerfeld modes is calculated, on the basis of a formal solution to the initial-value problem. The relevant timescale for the development of the perturbation is identified as a viscous one. Even so, the induced energy density can greatly exceed that associated with the initial normal velocity, before decay sets in. Initial conditions corresponding to the least-damped Orr–Sommerfeld mode induce the largest energy density and a maximum is obtained for structures infinitely elongated in the streamwise direction. In this limit, the asymptotic solution is derived and it shows that the spanwise wavenumbers at which the largest amplification occurs are 2.60 and 1.98, for symmetric and antisymmetric normal vorticity, respectively. The asymptotic analysis also shows that the propagation speed for induced symmetric vorticity is confined to a narrower range than that for antisymmetric vorticity. From a consideration of the neglected nonlinear terms it is found that the normal velocity component cannot be nonlinearly affected by the normal vorticity growth for structures with no streamwise dependence.

1. Introduction

In the traditional analysis of the laminar-to-turbulent transition for wall-bounded parallel shear flows, the primary instability is assumed to be a two-dimensional Tollmien–Schlichting wave, with three-dimensionality only entering at the secondary-instability level. This model has been quite successful in explaining many features of vibrating-ribbon experiments (see Herbert 1983, 1988, for reviews) but other experiments have suggested the possibility of 'by-pass' mechanisms to transition, not involving two-dimensional Tollmien–Schlichting waves (Morkovin 1978). These would operate in, for example, pipe flow, in the spanwise spreading of turbulent regions in boundary layers, in transition due to distributed roughness and in high-noise environments.

In experiments where localized disturbances are introduced into the flow, turbulence first appears as turbulent spots without the appearance of two-

dimensional Tollmien–Schlichting waves. In fact, Chambers & Thomas (1983) found that a turbulent spot in a boundary layer does not seem to interact with a large-amplitude two-dimensional Tollmien–Schlichting wave. This indicates that the propagation and maintenance of turbulent spots may be associated directly with three-dimensional processes. However, *oblique* Tollmien–Schlichting waves have been observed at the turbulent spots in wing-tip boundary layers (Wygnanski, Haritonidis & Kaplan 1979) and in plane Poiseuille flow (Carlson, Widnall & Peeters 1982 and Alavyoon, Henningson & Alfredsson 1986), but they are not present in water table flow (Lindberg *et al.* 1984). Since these waves are not present in all flow situations, it is doubtful whether they are primarily associated with a generic mechanism for the maintenance of spots. It seems therefore worthwhile to consider other aspects of the three-dimensional problem.

In linear theory, the development of two-dimensional disturbances is completely described by the modes of the Orr–Sommerfeld equation, but for three-dimensional disturbances a second equation is required for a full description of the flow field. Most conveniently, this equation is that for the vorticity perturbation normal to the wall. Its homogeneous part involves the Squire modes, which are damped (Davey & Reid 1977), so it is tempting to neglect the importance of these modes in the development of three-dimensional disturbances. However, the normal vorticity is *forced* by the normal velocity and the possibility of algebraic growth has been recognized.

In the inviscid case, Ellingsen & Palm (1975) showed that the streamwise velocity component of a small three-dimensional disturbance with no streamwise variation grows linearly with time. And in a related work, Landahl (1980) deduced that the streamwise integrated kinetic energy grows at least linearly in t, as $t \to \infty$, provided that the net initial momentum normal to the wall is non-zero.

For the viscous flow in a boundary layer, initial algebraic growth of infinitely elongated structures has been found to be associated with the continuous spectrum of the Orr–Sommerfeld equation (Hultgren & Gustavsson 1981). It is then a special case of a direct resonance between the normal vorticity and the normal velocity components. In bounded flows, this mechanism has also been found to be present for waves oblique to the mean flow (Gustavsson & Hultgren 1980 and Gustavsson 1981). But a study of plane Poiseuille flow (Gustavsson 1986) seems to reduce the role of the explicit algebraic time-dependence obtained at a direct resonance. However, the work was not concerned with the complete solution of the initial-value problem and a reassessment of the results shows that algebraic growth may be possible if the full problem is considered.

Therefore, a more detailed investigation is made in the present paper on the character of the forcing of normal vorticity by normal velocity. The study is based on the complete solution of the linear initial-value problem in plane Poiseuille flow. In §2, the analytical foundation is given. Relevant equations for developing three-dimensional disturbances, and the boundary conditions, are reiterated in §2.1 and the formal solution for the normal vorticity is given in Appendix A. The kinetic energy density, in the wavenumber plane, of the induced vorticity is used to characterize the response to the forcing and it is defined in §2.2. Since only the induced normal vorticity is of interest here, the initial vorticity is set to zero and in §2.3, general expressions for flow fields satisfying this condition are presented. An arbitrary disturbance of the normal velocity can be expressed as a sum of Orr–Sommerfeld modes, but only the forcing by individual modes is studied. In Appendix B is shown how the formal solution of the initial-value problem for the normal velocity is reduced if the initial data correspond to an eigenfunction of the

Orr–Sommerfeld equation. The resulting solution for the induced normal vorticity is derived in §2.4.

The results point to the importance of structures infinitely elongated in the streamwise direction, the analytical solutions for which are given in Appendix C, together with the asymptotic results for propagation speeds. As a substantial growth of the kinetic energy density is obtained, the consequences for developing disturbances in physical space are also considered. In particular, the Reynolds-number effect is discussed as well as some experimental implications. Finally, the character of nonlinear effects is briefly discussed.

2. Analysis

2.1. *Equations and boundary conditions*

Consider a plane Poiseuille flow for $|y| < 1$. The mean flow, $U(y) = 1-y^2$, is in the x-direction and z is the spanwise coordinate. The development of a small three-dimensional disturbance (u, v, w) to this flow is governed by an equation for the normal velocity, v, and one of the normal vorticity, $\omega = (\partial u/\partial z) - (\partial w/\partial x)$, which in non-dimensional form read

$$\left(\frac{\partial}{\partial t} + U\frac{\partial}{\partial x}\right)\nabla^2 v - U''\frac{\partial v}{\partial x} = \frac{1}{R}\nabla^4 v \tag{1}$$

and

$$\left(\frac{\partial}{\partial t} + U\frac{\partial}{\partial x}\right)\omega - \frac{1}{R}\nabla^2\omega = -U'\frac{\partial v}{\partial z}, \tag{2}$$

where prime denotes a y-derivative and ∇^2 is the three-dimensional Laplacian. $R(= U_0 h/\nu)$ is the Reynolds number, where h is the channel half-width, U_0 the centreline velocity and ν the kinematic viscosity. The boundary conditions for v and ω are

$$v = \frac{\partial v}{\partial y} = \omega = 0 \quad \text{at} \quad y = \pm 1. \tag{3a–c}$$

Given the initial conditions for v (actually $\nabla^2 v$) and ω, formal solutions to (1) and (2) can be obtained using Fourier transformation in the homogeneous coordinates x and z and Laplace transformation in time. The solution for v has been given in plane Poiseuille flow by Shanthini (1989), and for ω in plane Couette flow by Gustavsson & Hultgren (1980). The latter solution is readily adapted to the case of plane Poiseuille flow and is given in Appendix A, for reference.

2.2. *The kinetic energy density*

The kinetic energy of the perturbation field is given by

$$T = \frac{1}{2}\int_x\int_y\int_z (u^2+v^2+w^2)\,\mathrm{d}x\,\mathrm{d}y\,\mathrm{d}z, \tag{4}$$

which in Fourier space may be rewritten as (cf. Gustavsson 1986)

$$T = \frac{1}{2}\int_\alpha\int_\beta\int_y \frac{1}{k^2}(|\hat{\omega}|^2 + k^2|\hat{v}|^2 + |\mathrm{D}\hat{v}|^2)\,\mathrm{d}y\,\mathrm{d}\alpha\,\mathrm{d}\beta, \tag{5}$$

where the circumflex denotes Fourier transformation, with transform variables α and β. Also, $k^2 = \alpha^2 + \beta^2$ and $\mathrm{D} = \mathrm{d}/\mathrm{d}y$. If the α and β integrations are omitted in (5), the *energy density* in the (α, β)-plane is obtained,

$$e = \frac{1}{2}\int_y \frac{1}{k^2}(|\hat{\omega}|^2 + k^2|\hat{v}|^2 + |\mathrm{D}\hat{v}|^2)\,\mathrm{d}y. \tag{6}$$

2.3. *Flow fields with zero normal vorticity*

The main concern of this paper is to investigate the forcing of ω by v. Therefore, the initial vorticity, ω_0, is set to zero and the term ψ_{init} in (A 1) in Appendix A thus vanishes. The remaining term, ψ_{ind}, corresponds to a perturbation which is zero at $t = 0$, a fact which may be used as a check of numerical calculations. The character of flow fields with zero normal vorticity can be deduced by considering the horizontal velocity components. For such flows, continuity gives

$$\hat{u}_0 = \frac{\mathrm{i}\alpha}{k^2}\frac{\partial \hat{v}_0}{\partial y} \quad \text{and} \quad \hat{w}_0 = \frac{\mathrm{i}\beta}{k^2}\frac{\partial \hat{v}_0}{\partial y}, \tag{7a, b}$$

where subscript zero indicates values at $t = 0$. Application of the convolution theorem for Fourier transforms leads then to the following expressions for u_0 and w_0:

$$u_0(x, y, z) = -\frac{1}{2\pi}\int_{-\infty}^{\infty}\int_{-\infty}^{\infty}\frac{x-\xi}{r'^2}\frac{\partial v_0}{\partial y}\,\mathrm{d}\xi\,\mathrm{d}\zeta, \tag{8a}$$

and

$$w_0(x, y, z) = -\frac{1}{2\pi}\int_{-\infty}^{\infty}\int_{-\infty}^{\infty}\frac{z-\zeta}{r'^2}\frac{\partial v_0}{\partial y}\,\mathrm{d}\xi\,\mathrm{d}\zeta, \tag{8b}$$

where $r'^2 = (x-\xi)^2 + (z-\zeta)^2$ and $v_0 = v_0(\xi, y, \zeta)$. In the special case when v_0 is axisymmetric in the (ξ, ζ)-plane, i.e. depends only on y and $\rho = (\xi^2 + \zeta^2)^{\frac{1}{2}}$, the azimuthal velocity in this plane is zero and the radial velocity, u_r, becomes

$$u_r = -\frac{1}{r}\int_0^r \rho'\frac{\partial v_0}{\partial y}\,\mathrm{d}\rho'. \tag{9}$$

This can be deduced from (8), or directly from continuity. Integration of (9) in the y-direction shows that the common experimental condition of a jet-like inflow normal to the wall is consistent with a flow field with zero normal vorticity.

2.4. *Solution for the normal vorticity excited by one Orr–Sommerfeld mode*

Since a general v-disturbance can be expressed as a sum of the modes of the Orr–Sommerfeld (O–S) equation, it is natural to study the induced vorticity from individual modes. It is then a simple matter of superposition to obtain the response from combinations of modes as would be required if the y-distribution of the initial v-disturbance is arbitrary. In Appendix B, it is shown how the general solution to the initial-value problem for v reduces when the initial v is an eigenfunction of the O–S equation. If $\bar{\phi}$ is the eigenfunction, and $\bar{\sigma}$ the eigenvalue, the result for the Fourier–Laplace transform of $v(\equiv \phi)$ becomes

$$\phi = -\frac{\bar{\phi}}{(\sigma - \bar{\sigma})}R. \tag{10}$$

A normal velocity perturbation generates normal vorticity of opposite symmetry,

and using (A 3) the following expression for the induced normal vorticity is obtained if $\bar{\phi}$ is antisymmetric:

$$\frac{\psi_s}{R} = \frac{i\beta R}{\sigma-\bar{\sigma}}\left\{\psi_1(y)\frac{1}{\psi_{11}}\int_0^1 U'\bar{\phi}_a[\psi_{21}\psi_1(\eta)-\psi_{11}\psi_2(\eta)]\,d\eta + \int_0^y U'\bar{\phi}_a[\psi_1(y)\psi_2(\eta)-\psi_2(y)\psi_1(\eta)]\,d\eta\right\}, \quad (11)$$

where the subscripts s and a indicate symmetric and antisymmetric, respectively. ψ_1 and ψ_2 satisfy the equation

$$\psi''-[k^2+i\alpha RU-\sigma]\psi = 0, \quad (12)$$

and are normalized such that $\psi_1 = \psi_2' = 1$ and $\psi_1' = \psi_2 = 0$ at $y = 0$. (As the other symmetry case is analogous, only one case is considered in detail.)

To obtain the explicit time-dependence for $\hat{\omega}_s$, the Laplace transform in (11) must be inverted. The inverse is obtained by the appropriate choice of integration contour in the complex s-plane, but since s is related to the variable σ through

$$\sigma = -Rs, \quad (13)$$

the inverse is, instead, evaluated in the complex σ-plane. Then,

$$\hat{\omega}_s = \frac{1}{2\pi i}\int_{\Gamma_\sigma} e^{-\sigma t/R}\frac{\psi_s(\sigma)}{R}d\sigma, \quad (14)$$

where Γ_σ is the inversion contour. To obtain $\hat{\omega}_s$ is thus only a matter of identifying the poles in the right-hand side of (11). The induced normal vorticity will consist of two parts, one associated with the pole at $\sigma = \bar{\sigma}$ (the forcing frequency) and the other due to the poles $\psi_{11} = 0$. The residue value for the first case is directly obtained as $i\beta R\, e^{-\bar{\sigma}t/R}$ times the terms in curly brackets in (11), evaluated for $\sigma = \bar{\sigma}$. For the other poles, the residue at a pole σ_n involves the value of $\partial\psi_{11}/\partial\sigma$ at $\sigma = \sigma_n$, since $\psi_{11} = (\sigma-\sigma_n)\,\partial\psi_{11}/\partial\sigma$ close to the pole. Differentiation of (12) with respect to σ gives the following equation for $\partial\psi_1/\partial\sigma$:

$$\frac{\partial\psi_1''}{\partial\sigma}-[k^2+i\alpha RU-\sigma]\frac{\partial\psi_1}{\partial\sigma} = -\psi_1, \quad (15)$$

the homogeneous solutions of which are identical to those of (12). By using variation of the parameters, the solution to (15) thus becomes

$$\frac{\partial\psi_1}{\partial\sigma} = \psi_1(y)\int_0^y \psi_1\psi_2\,d\eta-\psi_2(y)\int_0^y \psi_1^2\,d\eta. \quad (16)$$

At $y = 1$, where $\psi_{11} = 0$, (16) gives

$$\frac{\partial\psi_{11}}{\partial\sigma} = -\psi_{21}\int_0^1 \psi_1^2\,dy, \quad (17)$$

and the residue at such a pole becomes

$$-i\beta R\frac{e^{-\sigma_n t/R}}{\sigma_n-\bar{\sigma}}\psi_{1n}(y)\frac{\int_0^1 U'\bar{\phi}_a\psi_{1n}\,dy}{\int_0^1 \psi_{1n}^2\,dy}. \quad (18)$$

In the Fourier plane, the induced (symmetric) normal vorticity can thus be written as

$$\hat{\omega}_s = \mathrm{i}\beta R\, \mathrm{e}^{-\bar{\sigma}t/R}\{\ldots\}_{\sigma=\bar{\sigma}} - \mathrm{i}\beta R \sum_n \frac{\mathrm{e}^{-\sigma_n t/R}}{\sigma_n - \bar{\sigma}} \psi_{1n}(y) \frac{\int_0^1 U' \bar{\phi}_a \psi_{1n}\, \mathrm{d}y}{\int_0^1 \psi_{1n}^2\, \mathrm{d}y}, \tag{19}$$

using obvious notation. A condensed and quite elegant form of (19), originally derived by Henningson (1990) through a direct approach to the expansion problem for the normal vorticity, can be obtained by noting that $\hat{\omega}_s$ is zero at $t/R = 0$. Thus,

$$\{\ldots\}_{\sigma=\bar{\sigma}} = \sum_n \frac{1}{\sigma_n - \bar{\sigma}} \psi_{1n}(y) \frac{\int_0^1 U' \bar{\phi}_a \psi_{1n}\, \mathrm{d}y}{\int_0^1 \psi_{1n}^2\, \mathrm{d}y}, \tag{20}$$

which can be substituted into (19) to give the final expression

$$\hat{\omega}_s = -\mathrm{i}\beta R \sum_n \frac{\mathrm{e}^{-\bar{\sigma}t/R} - \mathrm{e}^{-\sigma_n t/R}}{\bar{\sigma} - \sigma_n} \psi_{1n}(y) \frac{\int_0^1 U' \bar{\phi}_a \psi_{1n}\, \mathrm{d}y}{\int_0^1 \psi_{1n}^2\, \mathrm{d}y}. \tag{21}$$

(The other symmetry case is obtained by changing $\bar{\phi}_a$ to $\bar{\phi}_s$ and ψ_{1n} to ψ_{2n}.)

The solution (21) shows that the relevant time parameter for the development of a disturbance is t/R and the proper timescale is thus the viscous scale h^2/ν. From (21) the algebraic t/R-dependence for small times follows immediately, if the exponential terms are Taylor-expanded. Also, the algebraic t/R-dependence which appears at a direct resonance ($\bar{\sigma} = \sigma_n$, some n) is readily obtained.

Aside from the explicit t/R-dependence, the sum in (21) is characterized by the two parameters k and αR so, because of the βR-factor, three parameters need to be specified for $\hat{\omega}$ to be calculated. Most conveniently, these are k, αR and R. Then, βR may be written as

$$\beta R = k(R^2 - (\alpha R/k)^2)^{\frac{1}{2}}. \tag{22}$$

With this choice of parameters, it is straightforward to apply the results obtained at one Reynolds number to other R-values. Since R appears only in the βR-factor in (21) the amplitude effect on $\hat{\omega}$ of changes in R and with k and αR fixed is easily determined. However, with αR fixed, an increase in R will decrease α, and vice versa. Also, β will vary according to (22) so new (α, β)-values will be associated with the rescaled amplitude of $\hat{\omega}$. From these considerations some general conclusions can be drawn about the behaviour of $\hat{\omega}$ as R is changed. For increasing R, βR tends to kR so $\hat{\omega}$ becomes proportional to R. (When $\alpha R = 0$, strict proportionality in R applies at all Reynolds numbers.) Similarly, the energy density associated with the normal vorticity, as given in (6), will in view of (22) be weighted by a factor $R^2 - (\alpha R/k)^2$, and thus scales with R^2 as $R \to \infty$. Also, $\alpha \to 0$, which corresponds to structures increasingly elongated in the streamwise direction.

As R decreases, β becomes zero when $R = \alpha R/k$. This corresponds to a two-dimensional disturbance, for which the normal vorticity is zero.

It should be remarked that the R-dependence is a unique property of the induced normal vorticity and has no counterpart in the normal velocity; the R-factor in (10) will not show up explicitly when inverting the Laplace transform, according to (14).

Finally, it must be remembered that the R-dependence discussed applies only in wavenumber space; the consequences in physical space are considered in the discussion.

3. Numerical results

3.1. *Normalization of the forcing O–S mode*

For each combination of $(k, \alpha R)$ the O–S equation produces an infinite number of eigenmodes and in the parameter range studied all modes are damped. The amplitude of a single forcing O–S mode was chosen such that its initial energy density is unity, i.e.

$$\int_0^1 \{|\bar{\phi}|^2 + \frac{1}{k^2}|\mathrm{D}\bar{\phi}|^2\}\,\mathrm{d}y = 1. \tag{23}$$

Owing to the damping, the corresponding integral with $\hat{v}$ will thus be less than unity for $t > 0$.

3.2. *Numerical techniques*

The numerical study started with the determination, at a given $(k, \alpha R)$, of the eigenmodes of the O–S equation. The eigenvalues were determined by a shooting method, and a fourth-order Adams implicit method was used to integrate the O–S equation. The eigenfunction was then normalized according to (23), where the numerical quadrature was done with the Simpson rule, extended with three steps of Richardson extrapolation, thus producing an error of $O(\Delta y^{10})$, where Δy is the step size. This method requires the number of steps to be a factor of 12, and typically 432 steps were used. Then, a number of vorticity modes were determined, and the normal vorticity resulting from the forcing frequency, and a sum of terms like (18), was calculated at 36 (= 432/12) steps. Strictly, an infinite number of residues of the form (18) should be added to the residue at $\sigma = \bar{\sigma}$ in order to represent the vorticity. However, it was found that, as the damping of the individual vorticity modes became larger than that of the forcing O–S mode, addition of further modes only acted to improve the accuracy at $t/R = 0$ and typically only six vorticity modes were required to resolve the essential features of the time development. The simpler expression (21) was also used to give an independent verification of the calculations. Finally, the energy density of the normal vorticity,

$$\frac{1}{k^2}\int_0^1 |\hat{\omega}|^2\,\mathrm{d}y, \tag{24}$$

was determined for various values of t/R.

3.3. *General behaviour of the induced energy density*

For $k = 1$ and $\alpha R = 100$, the time dependence of (24) was determined for the two least-damped O–S modes, normalized according to (23), and the results are shown in figure 1. The Reynolds number chosen was 1000, but the amplitude can easily be rescaled to other Reynolds numbers using (22).

Figure 1 exhibits the general time behaviour of the induced energy density: it starts at zero for $t/R = 0$, increases to a maximum and then decays to zero. In the decaying part the major contribution comes from the least-damped mode, but in the growth phase more modes are important. For small times, the energy density is proportional to $(t/R)^2$ since the normal vorticity grows like t/R. Figure 1 also shows

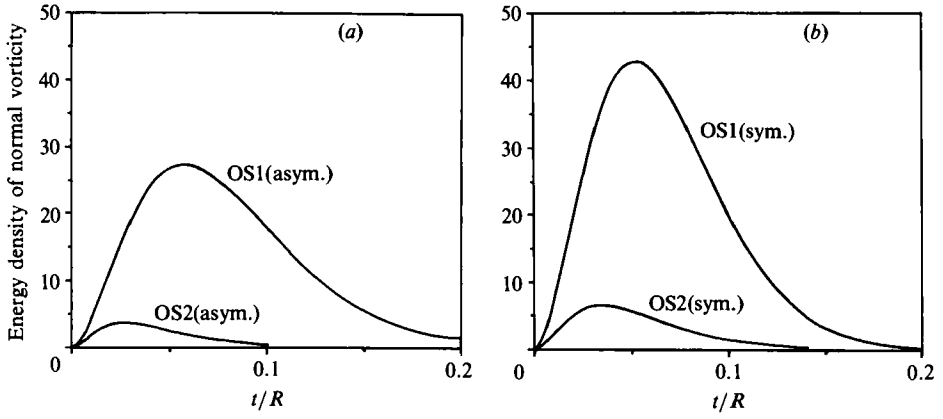

FIGURE 1. Development of the energy density for the normal vorticity induced by the two least-damped O–S modes (OS1 and OS2). ($R = 1000$, $k = 1$, $\alpha R = 100$). (*a*) Symmetric vorticity (antisymmetric O–S); (*b*) antisymmetric vorticity (symmetric O–S).

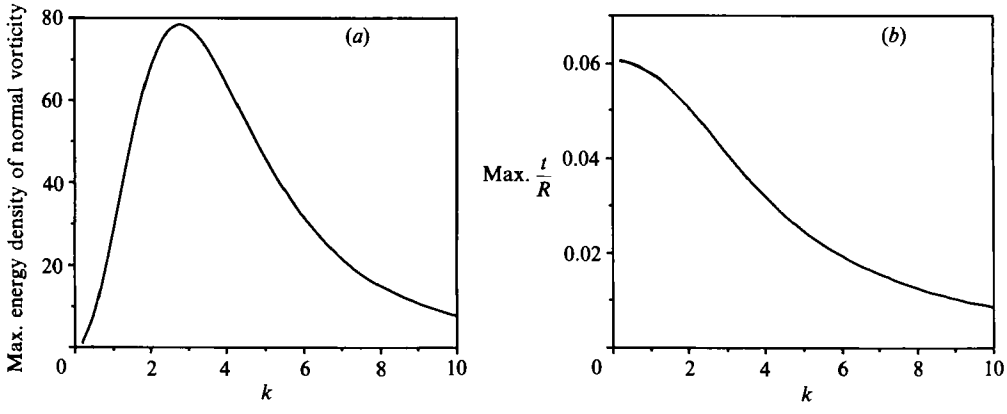

FIGURE 2. (*a*) Maximum energy density in figure 1 (*a*) symmetric vorticity) for various k; (*b*) t/R-values for the points in (*a*). ($R = 1000$, $\alpha R = 100$).

that the least-damped O–S mode induces the largest energy density at any given time. This was found to be a general property so further investigation was concentrated on the least-damped O–S mode for each symmetry case. For the least-damped antisymmetric O–S mode, keeping αR fixed ($= 100$) and varying k, the maximum amplitude of figure 1 and the time to reach the maximum were determined and are shown in figure 2. Since the maximum occurs at different t/R, for various k, a more detailed diagram would show contours of the energy density as a function of k and t/R. However, each αR produces one such diagram so the effect of changing αR was considered next. This showed that a larger αR produces a smaller value at the peak compared to that in figure 2 (*a*), with k slightly varying from the value in that figure. But for smaller αR, larger maxima were obtained. For this case the analytical solutions were therefore derived and are given in Appendix C.

3.4. *Results for* $\alpha R = 0$

3.4.1. *Energy density of induced normal vorticity*

The energy density of the normal vorticity, represented by (C 9) and (C 17) in Appendix C, was calculated for various k-values with the least-damped O–S mode as the forcing. The results are summarized in figure 3 where the contours of the energy

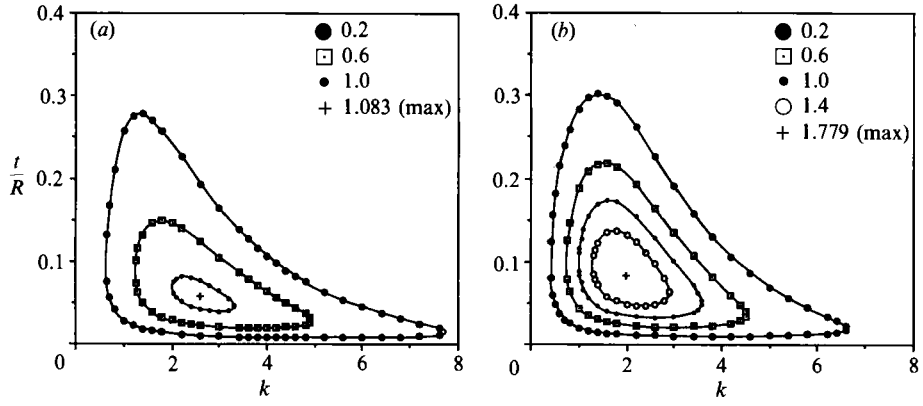

FIGURE 3. Contour curves in the $(k, t/R)$-plane for the energy density, in units of $10^{-4} \times R^2$, of the normal vorticity induced by the least-damped O–S mode. (*a*) Symmetric vorticity; (*b*) antisymmetric vorticity. ($\alpha R = 0$).

Case	Forcing mode	k(peak)	t/R(peak)	(peak value)$/R^2$
Symmetric vorticity	OS1	2.60	0.0572	1.083×10^{-4}
	OS2	4.11	0.0182	1.441×10^{-5}
	OS3	5.88	0.00853	3.314×10^{-6}
Antisymmetric vorticity	OS1	1.98	0.0840	1.779×10^{-4}
	OS2	3.18	0.0309	3.748×10^{-5}
	OS3	4.95	0.0121	6.523×10^{-6}

TABLE 1. Characteristics of the peak values of induced energy density from forcing by different O–S modes. The forcing O–S modes have opposite symmetry to the vorticity modes. $\alpha R = 0$

density, in units of $10^{-4} \times R^2$, are plotted as a function of k and t/R. The contours show some noteworthy features. First, there is a maximum value at a certain combination of k and t/R. These values are 1.083 for symmetric vorticity and 1.779 for antisymmetric, and are located at $k = 2.60$, $t/R = 0.0572$ and $k = 1.98$, $t/R = 0.0840$, respectively. For a k-value to the right of the peak, the t/R-dependence is more compressed than to the left, indicating that shorter spanwise scales are most quickly damped. Conversely, for a given t/R, the k-dependence is seen to be more compressed above the peak. The extension of the contours below the peak indicates that initially a wide spectrum of spanwise scales is subject to growth. As the peak is passed, a narrower k-range is amplified, with a slight shift of the k with maximum growth towards smaller values. This shift is largest for symmetric vorticity. Differences in the particular shape of the contours are also evident from the figures.

For initial conditions corresponding to higher O–S modes, the character of the contours is similar to those of figure 3, but the peak amplitude and its position in the $(k, t/R)$-plane is changed. The essential data are summarized in table 1 from which it can be seen that even the third O–S mode is capable of producing growth at $R = 1000$.

3.4.2. *Phase speeds*

The phase speed, c_0, of the least-damped O–S mode, as given by (C 6) and (C 16), was calculated for $0.2 < k < 10$ and the results are shown in figure 4. For the antisymmetric mode, c_0 is seen to vary only slightly with k and is in the interval

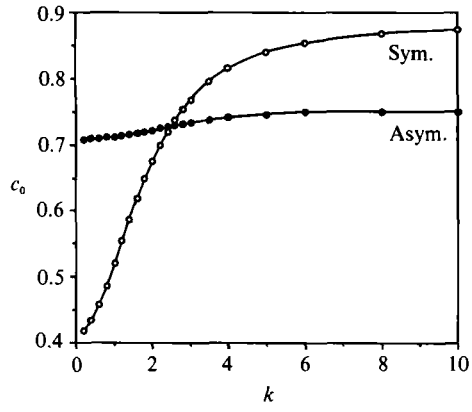

FIGURE 4. Phase speed of least-damped O–S mode at various k and at $\alpha R = 0$: ○, symmetric mode; ●, antisymmetric mode.

0.71–0.75. In contrast, c_0 for the symmetric mode varies considerably and is in the interval 0.42–0.87.

The phase speeds, c_n, of the vorticity modes are given by (C 12), where γ_n is given by (C 8) for symmetric modes, and by (C 18) for antisymmetric modes. In the former case, $c_n = 0.87, 0.69, 0.67$ for the first three modes and for the latter case, $c_n = 0.72, 0.68, 0.67$. In both cases, c_n approaches $\frac{2}{3}$ for the higher modes.

Since both the forcing O–S mode and the vorticity modes determine the speed of the induced normal vorticity, it can be concluded that the propagation speed for symmetric vorticity is confined to a narrower range than for antisymmetric vorticity.

3.4.3. *y-Distribution of induced normal vorticity*

The development of the induced kinetic energy density was obtained by integrating the vorticity distribution in the y-direction so it was considered of some interest to study also the temporal development of the y-distribution of the vorticity. This was done for k-values at the peaks in figure 3 and the results are presented in figure 5. It is seen that, for antisymmetric vorticity (figure 5*b*), the amplitude at maximum energy density ($t/R = 0.084$) is largest for all y-values. For symmetric vorticity, however, the temporal evolution of the y-distribution, and its relation to maximum energy density, is more complicated. The vorticity distribution is seen to develop a maximum which eventually moves towards the centreline as its magnitude decreases. Consequently, the amplitude can locally be larger than at maximum energy density ($t/R = 0.0572$), but the maximum amplitude of the vorticity (≈ 0.037), obtained at the time of maximum energy density, is never exceeded anywhere at any other time. The results show that the temporal development of the local vorticity close to the centreline may not be directly related to the development of the energy density in this case.

3.5. *Results for* $\alpha R \neq 0$

3.5.1. *Growth region in the* (α, β)*-plane*

Even if the largest amplitude is obtained at $\alpha R = 0$, growth is also present for other αR-values (figure 2*a* shows the results at $\alpha R = 100$ and $k = 1$). Although a thorough investigation of the extent of the growth region is the subject for a separate study, an example is presented in figure 6. The figure shows contours in the (α, β)-

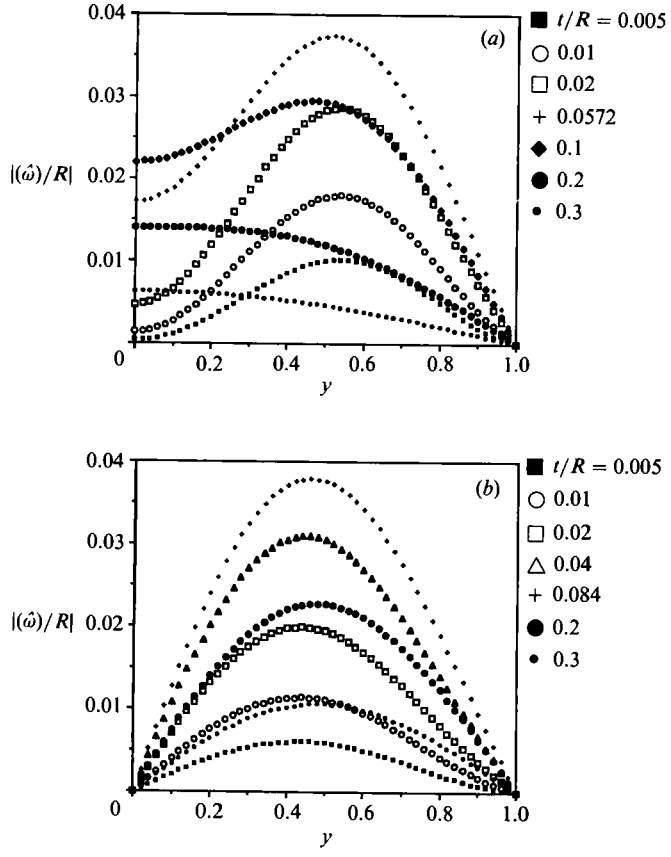

FIGURE 5. y-Distribution of absolute value of normal vorticity, in units of R, at various t/R-values. ($\alpha R = 0$). (*a*) Symmetric vorticity ($k = 2.60$), (*b*) antisymmetric vorticity ($k = 1.98$).

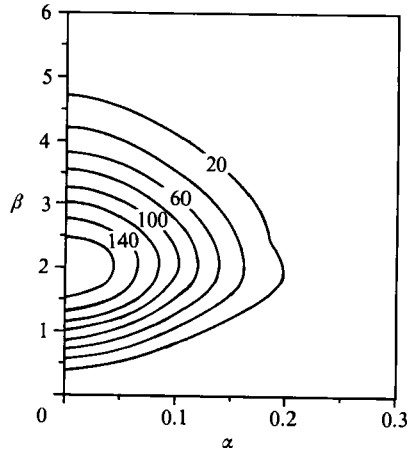

FIGURE 6. Contour curves in the (α, β)-plane for energy density of induced normal (antisymmetric) vorticity. The labels are values of the energy density (distance between contours is 20, $t/R = 0.08$, $R = 1000$).

plane of the induced energy density of antisymmetric normal vorticity at $R = 1000$ and $t/R = 0.08$, which is close to the time when the peak value for $\alpha R = 0$ is reached. A phenomenon of special interest is exhibited in this figure by the contour with the value 20. At the largest α-values, this curve has a slight indentation which is due to the two least-damped O–S modes coinciding at $k = 2.539$ and $\alpha R = 216.6$ (cf. Shanthini 1989), which is just outside the distorted contour. As the extension of the growth region is larger for smaller times, but with a lower peak value, the degeneracy will influence the shape of the contours primarily in the initial phase. A proper assessment of the induced energy density for small times will therefore have to incorporate the two least-damped O–S modes. In particular, the generalized eigenfunction (Shanthini 1989) need to be considered at the degeneracy point.

Figure 6 is obtained for $R = 1000$ but, using the arguments of § 2.4, the relationship to contours at other R-values can be deduced quite easily. The argument rests upon the observation that $R \gg \alpha R/k$ in the region with substantial growth. Then, the induced energy density is approximately proportional to R^2 and a doubling of R, say, will quadruple the value on the contours. However, the rescaled values are associated with halved α-values, whereas β is marginally changed. Thus, figure 6 can be used at $R = 2000$ by simply multiplying the values on the contours by a factor 4 and rescaling the α-axis to the range 0–0.15.

3.5.2. *Direct resonance*

Since the direct resonance between the normal vorticity and velocity components originally motivated the present study, the growth properties of this mechanism were also investigated. It was observed that the energy density of the induced normal vorticity varied smoothly as the parameters k and αR varied across a resonance point and thus the temporal development follows the general behaviour of figure 3. Also, the direct resonances involve higher O–S modes, suggesting that only a small growth is possible. However, some of the direct resonances in Gustavsson (1986) do exhibit amplification. At $R = 1000$, resonance 2s ($k = 5.794$, $\alpha R = 145.1$) gave 16.5 times the initial energy density, 6s ($k = 1.015$, $\alpha R = 345.8$) 1.8 times and 1a ($k = 1.478$, $\alpha R = 116.1$) 2.8 times.

4. Discussion

The results presented show that amplification of the kinetic energy density of a small velocity perturbation can be obtained at sub-transitional Reynolds numbers by the mechanism of vortex stretching, operating on the normal vorticity component. It is an intriguing result that, although both the normal vorticity and the normal velocity components are expressed in terms of damped modes, considerable amplitudes can be reached before the decay sets in.

The growth pertains to wavenumber space, so it is important to assess its consequences in real space also. The kinetic energy, the normal vorticity and the associated velocity amplitudes are then quantities of primary concern, and of particular interest is their Reynolds-number dependence. In order to study this, the initial conditions need to be specified. Generally, these are given as distributions in the (α, β)-plane and it seems natural to base the argument on the growth properties in this plane. However, for a point disturbance in the (x, z)-plane the distribution in the (α, β)-plane is a constant and, since a distributed disturbance in the (x, z)-plane may be considered as a superposition of point disturbances, such a distribution may be assumed without loss of generality. With this choice, the fact that it is the

parameters k, αR and R (with variables t/R and y) that describe the induced normal vorticity can be fully exploited. Specifically, $\hat{\omega}$ can be written as

$$\hat{\omega} = -\mathrm{i}\beta R\hat{\Omega}(k, \alpha R; t/R, y), \tag{25}$$

where $\hat{\Omega}$ is related to the sum in (21). The induced kinetic energy can be determined from (5) via integration in the (α, β)-plane of the energy density. But, because of the specific parameter combination and the choice of initial distribution, the integration may equally be performed in the $(k, \alpha R)$-plane. The connection between integrations in the two planes is given by

$$\int_\alpha \int_\beta \ldots \mathrm{d}\alpha\, \mathrm{d}\beta = \int_k \int_{\alpha R} \ldots J\, \mathrm{d}k\, \mathrm{d}(\alpha R), \tag{26}$$

where $J(=-k/\beta R)$ is the Jacobian of the coordinate transformation. Here, integration covers the whole (α, β)-plane but, because $|\alpha| \leqslant k$, it is restricted to $|\alpha R| \leqslant kR$, $0 \leqslant k < \infty$, in the $(k, \alpha R)$-plane.

The kinetic energy for the induced normal vorticity becomes

$$T = \int_k \int_{\alpha R} [R^2 - (\alpha R/k)^2]^{\frac{1}{2}} \left(\int_0^1 |\hat{\Omega}|^2\, \mathrm{d}y \right) \mathrm{d}k\, \mathrm{d}(\alpha R), \tag{27}$$

and since the largest amplitudes are obtained when $R \gg \alpha R/k$, T is seen to be approximately proportional to R. However, when R increases, the integration region in the $(k, \alpha R)$-plane becomes larger and there is an additional contribution to the integral. To estimate this, more detailed information about the behaviour of $\hat{\Omega}$ is required.

The magnitude in real space of the normal vorticity is obtained by inverting the Fourier transform, and the following expression is obtained:

$$\omega = \frac{1}{2\pi} \int_k \int_{\alpha R} \mathrm{i}k \exp\left[\mathrm{i}\left(\alpha R \frac{x}{R} + \beta z \right) \right] \hat{\Omega}\, \mathrm{d}k\, \mathrm{d}(\alpha R), \tag{28}$$

where

$$\beta = k\left[1 - \frac{1}{R^2} \left(\frac{\alpha R}{k} \right)^2 \right]^{\frac{1}{2}}.$$

In (28), R appears only in β and since, again, $R \gg \alpha R/k$ in the region with largest growth, the R-dependence of ω seems to be weak. But, as for T, the integration region in the $(k, \alpha R)$-plane increases with R, which leads to an additional contribution to ω. In contrast to T, this contribution is non-zero at the boundary of the integration region ($\alpha R = kR$, or $\beta = 0$) so it is expected that the extra part could be relatively larger for ω than for T. Related to this is the observation that the region in the (k, αR)-plane where growth occurs is more extensive at small t/R-values (cf. figure 3 where $\alpha R = 0$). This indicates that the Reynolds-number effect on ω is more pronounced at earlier times than at later. Finally, it is observed from (28) that x/R appears as a natural lengthscale for the development of ω.

The results obtained can also be given an interpretation in terms of what can be expected in an experimental situation. The proper time parameter for the development of the normal vorticity is t/R, where t is the non-dimensional time based on U_0 and h. The dimensional time, t^*, thus becomes

$$t^* = t\frac{h}{U_0} = \frac{t}{R}\frac{h^2}{\nu}, \tag{29}$$

which shows that the time to reach the maximum in the vorticity is independent of

Reynolds number in an experiment where the fluid and the plate distance are kept constant. It may also be of interest to know the distance travelled when the largest amplitude occurs. The dimensional travel distance, L^*, for a disturbance is given by

$$L^* = c_R^* t^* = c_R U_0 \frac{t}{R} \frac{h^2}{\nu} = c_R \frac{t}{R} Rh, \tag{30}$$

where c_R is the (non-dimensional) propagation speed. This shows that the travel distance to reach the maximum in vorticity is proportional to R in a given experimental set-up and thus confirms the importance of the scaling educed from (28).

Of the particular quantitative results obtained, the spanwise scales, the propagation speeds and the time to reach maximum amplitude would be suitable for comparison with experiments. Also, the results that small streamwise wavenumbers are preferentially amplified should have experimental consequences. It suggests that streamwise streaky structures should develop from an initial disturbance. In discussions about streaky structures, the streamwise vorticity is often considered as an important quantity. However, the results obtained here do not support this conjecture. The streamwise vorticity of a perturbation is given by $(\partial w/\partial y)-(\partial v/\partial z)$ and, for streaky structures, continuity shows that $(\partial v/\partial y)+(\partial w/\partial z) \approx 0$. Thus, if v corresponds to a decaying disturbance, w will also decay and so does the streamwise vorticity. It seems therefore that only in a secondary, nonlinear phase can this vorticity component be dynamically significant. At the linear level considered here, the normal and the spanwise vorticity, $(\partial w/\partial x)-(\partial u/\partial y)$, components grow, and it may be an interesting object for further studies to determine the change of the vorticity vector due to this growth.

Experiments strictly pertaining to the assumptions of the theory presented here, i.e. small initial disturbances, are presently not available. However, the recent results by Klingmann & Alfredsson (1990) show that a disturbance generated by the injection of fluid through a hole in the wall, and which does not lead to a turbulent spot, develops in a manner which is consistent with the results obtained here.

In this context, it should be mentioned that the numerical simulations by Henningson, Johansson & Lundbladh (1989) showed that a streaky pattern develops from a localized initial disturbance consisting of two pairs of counter-rotating vortices. Also, the kinetic energy associated with the normal vorticity was found to have a considerable growth. Other numerical simulations (Kim & Moser 1989) have also established the growth of infinitely elongated structures.

Because of the growth, it is of considerable interest to know whether the mechanism studied can evoke nonlinear phenomena. As more work is needed to answer this, only a couple of aspects of the nonlinear problem will be discussed here. First, the results show that the growth of the normal vorticity is confined to a certain time interval. Therefore, it is likely that nonlinearities must come into play before the peak amplitudes have been passed. This gives $t/R = 0.084$ (cf. figure 3*b*) as the upper time limit before which nonlinear mechanisms must start to operate. This time applies to $\alpha = 0$, at which wavenumber the role of nonlinearity can be assessed in more detail. This is done by considering the nonlinear terms omitted in the derivation of (1) and (2). Following the notation in e.g. Benney & Gustavsson (1981), the nonlinear term in the v-equation is

$$\left(\frac{\partial^2}{\partial x^2}+\frac{\partial^2}{\partial z^2}\right) S_2 - \frac{\partial}{\partial y}\left(\frac{\partial S_1}{\partial x}+\frac{\partial S_3}{\partial z}\right), \tag{31}$$

where
$$S_i = u_j \frac{\partial u_i}{\partial x_j}, \tag{32}$$

using tensor notation. With $\partial/\partial x = 0$, (31) reduces to

$$\frac{\partial^2 S_2}{\partial z^2} - \frac{\partial^2 S_3}{\partial y \partial z}, \tag{33}$$

where
$$S_2 = v\frac{\partial v}{\partial y} + w\frac{\partial v}{\partial z}, \tag{34}$$

and
$$S_3 = v\frac{\partial w}{\partial y} + w\frac{\partial w}{\partial z}. \tag{35}$$

Continuity then also gives
$$\frac{\partial v}{\partial y} + \frac{\partial w}{\partial z} = 0. \tag{36}$$

As previously discussed, (36) shows that if v corresponds to a decaying mode, w will also decay. Thus, both S_2 and S_3 will decay and so does the nonlinear term (33). In linear theory, this term is neglected at $t = 0$, so it will always be small and nonlinear effects will not appear in v. This indicates that infinitely long structures may be dynamically passive in a nonlinear development, unless they form the basis for secondary instabilities. Thus, studies of nonlinear effects on the evolution of v through self-modulation by the present mechanism should therefore be directed to structures with $\partial/\partial x \neq 0$. However, for this case other approaches to the nonlinear problem are possible. One is to use the fact that the Fourier transform of a product is the convolution of the Fourier transforms for the individual factors. Applying this to (31), and eliminating u and w, produces among other terms the following vorticity–vorticity term:

$$\frac{\partial}{\partial y}\int_0^{2\pi}\int_0^{\infty} \frac{k'\sin^2(\theta-\varphi)}{1+(k'/k)^2-2(k'/k)\cos(\theta-\varphi)}\hat{\omega}(\alpha',\beta')\,\hat{\omega}(\alpha-\alpha',\beta-\beta')\,\mathrm{d}k'\,\mathrm{d}\varphi, \tag{37}$$

where $\alpha' = k'\sin\varphi$, $\beta' = k'\sin\varphi$, $\alpha = k\cos\theta$ and $\beta = k\sin\theta$. Since $\hat{\omega}$ is roughly proportional to R, it seems likely that this nonlinear term in real space is also proportional to R. Another large-Reynolds-number effect would therefore be to activate nonlinearity in the v-equation.

There are some obvious extensions of the present work such as a more detailed investigation of the energy growth in the (α,β)-plane and the y-dependence of the growth. Also, the properties of the nonlinear term (37) is an interesting topic for further studies. Finally, since the forcing mechanism studied is quite general, its capacity to amplify three-dimensional disturbances in other flows should be worth investigating. This particularly applies to flows which are predicted to be stable by traditional stability theory.

This work has in part been supported by the National Swedish Board for Technical Development (STU) through its program for basic research (STUF). The author has also benefited from discussions with Dr R. Shanthini and Professor D. Henningson.

Appendix A. Solution for the normal vorticity

Changing the limits of integration in the solution given in Gustavsson & Hultgren (1980), the solution for the Fourier–Laplace transform of the normal vorticity, ψ, is

$$\psi = \psi_{\text{init}} + \psi_{\text{ind}}, \tag{A 1}$$

where $\psi_{\rm init}(y) = -R\left(\frac{\chi_1(y)}{E}\int_{-1}^{1}\hat{\omega}_0\chi_2(\eta)\,\mathrm{d}\eta - \int_{-1}^{y}\hat{\omega}_0[\psi_1(y)\psi_2(\eta)-\psi_2(y)\psi_1(\eta)]\,\mathrm{d}\eta\right)$ (A 2)

and $\psi_{\rm ind}(y) = \mathrm{i}\beta R\left(\frac{\chi_1(y)}{E}\int_{-1}^{1}U'\phi\chi_2(\eta)\,\mathrm{d}\eta - \int_{-1}^{y}U'\phi[\psi_1(y)\psi_2(\eta)-\psi_2(y)\psi_1(\eta)]\,\mathrm{d}\eta\right).$ (A 3)

Here, $\hat{\omega}_0$ is the Fourier transform of the initial normal vorticity, ϕ the Fourier–Laplace transform of v,

$$\chi_1(y) = \psi_1(y)\psi_{2,-1} - \psi_2(y)\psi_{1,-1}, \tag{A 4}$$

$$\chi_2(y) = \psi_1(y)\psi_{2,1} - \psi_2(y)\psi_{1,1}, \tag{A 5}$$

and

$$E = \psi_{1,-1}\psi_{2,1} - \psi_{1,1}\psi_{2,-1}, \tag{A 6}$$

where ψ_1 and ψ_2 are solutions to equation (12). The second subscript indicates the y-value where the function is evaluated.

Appendix B. Solution of the initial-value problem for the normal velocity; eigenfunction excitation

Starting with the general solution for the normal velocity, as presented in Shanthini (1989), the initial value [$\Delta = (\mathrm{D}^2 - k^2)\hat{v}_0$] is split into antisymmetric and symmetric parts, but only the first case is studied in detail. The result for the symmetric case is then easily inferred. Thus,

$$\phi_{\rm a}(y;\sigma) = -R\left[F_{\rm ra}(y) + \frac{F_{24}(y)}{E_{24}}\right], \tag{B 1}$$

where

$$F_{\rm ra}(y) = \phi_1(y)\int_0^y K_1(\eta)\,\Delta_{\rm a}(\eta)\,\mathrm{d}\eta + \phi_3(y)\int_0^y K_3(\eta)\,\Delta_{\rm a}(\eta)\,\mathrm{d}\eta - \phi_2(y)\int_y^1 K_2(\eta)\,\Delta_{\rm a}(\eta)\,\mathrm{d}\eta - \phi_4(y)\int_y^1 K_4(\eta)\,\Delta_{\rm a}(\eta)\,\mathrm{d}\eta \tag{B 2}$$

and

$$F_{24}(y) = -\phi_2(y)\int_0^1 [E_{14}K_1(\eta) + E_{34}K_3(\eta)]\,\Delta_{\rm a}(\eta)\,\mathrm{d}\eta - \phi_4(y)\int_0^1 [E_{21}K_1(\eta) + E_{23}K_3(\eta)]\,\Delta_{\rm a}(\eta)\,\mathrm{d}\eta. \tag{B 3}$$

Here $\{\phi_\nu\}_{\nu=1}^4$ are the four linearly independent solutions to the O–S equation normalized such that

$$\left.\frac{\mathrm{d}^{n-1}\phi_\nu}{\mathrm{d}y^{n-1}}\right|_{y=0} = \delta_{n\nu} \quad (n = 1\ldots4). \tag{B 4}$$

$\{K_\nu\}_{\nu=1}^4$ are the cofactors of $\{\phi_\nu'''\}_{\nu=1}^4$ in the Wronskian for $\{\phi_\nu\}$ and can be shown to satisfy the adjoint to the O–S equation. They also satisfy the following relationships

$$\sum\phi_\nu K_\nu = \sum\phi_\nu K_\nu' = \sum\phi_\nu K_\nu'' = 0 \quad \text{and} \quad \sum\phi_\nu K_\nu''' = -1 \tag{B 5a–d}$$

Finally, $$E_{mn} = \phi_m \phi_n' - \phi_m' \phi_n \quad \text{at} \quad y = 1. \tag{B 6}$$

Assuming $\hat{v}_0$ to be an (antisymmetric) eigenfunction, $\bar{\phi}$, of the O–S equation with eigenvalue $\bar{\sigma}$, the initial condition becomes

$$\Delta_a = \bar{\phi}'' - k^2 \bar{\phi}. \tag{B 7}$$

The following relationship can then be used to simplify (B 2) and (B 3):

$$(\sigma - \bar{\sigma}) \int_0^y K(\bar{\phi}'' - k^2 \bar{\phi})\, \mathrm{d}y = [K\bar{\phi}''' - K'\bar{\phi}'' + K''\bar{\phi}' - K'''\bar{\phi} + (2k^2 + \mathrm{i}\alpha RU - \sigma)(K'\bar{\phi} - K\bar{\phi}') + \mathrm{i}\alpha RU' K\bar{\phi}]_0^y, \tag{B 8}$$

which holds if K satisfies the adjoint of the O–S equation, with parameter σ. (σ is related to the more commonly used phase speed, c, through $\sigma = \mathrm{i}\alpha Rc$). Applying (B 8) to (B 2), using (B 5) and the fact that $\bar{\phi} = \bar{\phi}' = 0$ at $y = 1$, leads to the following expression:

$$(\sigma - \bar{\sigma}) F_{ra}(y) = \bar{\phi}(y) - C_3[K_{21}\phi_2(y) + K_{41}\phi_4(y)] + C_2[K'_{21}\phi_2(y) + K'_{41}\phi_4(y)] \tag{B 9}$$

where $$C_2 = \bar{\phi}''(y = 1), \quad C_3 = \bar{\phi}'''(y = 1) \tag{B 10a, b}$$

and $$K_{21} = K_2(y = 1) \text{ etc.}$$

Similarly, for (B 3) is obtained

$$(\sigma - \bar{\sigma}) F_{24}(y) = -\phi_2(y)\{(E_{14}K_{11} + E_{34}K_{31})C_3 - (E_{14}K'_{11} + E_{34}K'_{31})C_2\} - \phi_4(y)\{(E_{21}K_{11} + E_{23}K_{31})C_3 - (E_{21}K'_{11} + E_{23}K'_{31})C_2\}. \tag{B 11}$$

From the definition of $\{K_\nu\}$ in terms of $\{\phi_\nu\}$, it is straightforward to show that the following relationships hold:

$$E_{14}K_{11} + E_{34}K_{31} + E_{24}K_{21} = 0, \quad E_{14}K'_{11} + E_{34}K'_{31} + E_{24}K'_{21} = 0, \tag{B 12a, b}$$

$$E_{21}K_{11} + E_{23}K_{31} + E_{24}K_{41} = 0, \quad E_{21}K'_{11} + E_{23}K'_{31} + E_{24}K'_{41} = 0. \tag{B 12c, d}$$

Using (B 12) in (B 11) then gives

$$(\sigma - \bar{\sigma}) \frac{F_{24}(y)}{E_{24}} = C_3[K_{21}\phi_2(y) + K_{41}\phi_4(y)] - C_2[K'_{21}\phi_2(y) + K'_{41}\phi_4(y)] \tag{B 13}$$

and the combination of (B 1), (B 9) and (B 13) finally produces

$$\phi_a(y; \sigma, \bar{\sigma}) = -\frac{\bar{\phi}(y; \bar{\sigma})}{(\sigma - \bar{\sigma})} R, \tag{B 14}$$

where the proper σ-dependences are shown explicitly.

Appendix C. Asymptotic results as $\alpha R \to 0$

The technique to obtain the asymptotic forms as $\alpha R \to 0$ is described in for example Drazin & Reid (1981, p. 159) and amounts to the following expansions for the eigenfunction to the O–S equation and the eigenvalue:

$$\bar{\phi} = \bar{\phi}_0 + \alpha R \bar{\phi}_1 + \ldots, \tag{C 1}$$

$$c = \frac{k^2 + \bar{\gamma}^2}{\mathrm{i}\alpha R} + c_0 + \alpha R c_1 + \ldots. \tag{C 2}$$

To order $(\alpha R)^0$, $\bar{\phi}_0$ and $\bar{\gamma}^2$ are determined, and to order $(\alpha R)^1$ the solvability condition gives c_0. The antisymmetric eigenfunction becomes

$$\bar{\phi}_{0a} = A[\sinh k \sin(\bar{\gamma} y) - \sin\bar{\gamma}\sinh(ky)], \tag{C 3}$$

where

$$A^2 = \frac{2k^2}{(\bar{\gamma}^2+k^2)(1-\sin 2\bar{\gamma}/2\bar{\gamma})} \tag{C 4}$$

is obtained from normalization of the energy and $\bar{\gamma}$ is determined from the dispersion relationship

$$k\tan\bar{\gamma} = \bar{\gamma}\tanh k, \tag{C 5}$$

from which $\bar{\gamma}$ can be calculated with iterative techniques.

The phase speed (c_0) becomes

$$c_0 = \left[\left(-\frac{3}{4}+\frac{k^2}{4\bar{\gamma}^2}+\frac{4\bar{\gamma}^2}{\bar{\gamma}^2+k^2}\right)\left(1-\frac{\sin(2\bar{\gamma})}{2\bar{\gamma}}\right)+\left(\frac{1}{\sinh^2 k}-\frac{1}{k\tanh k}\right)\sin^2\bar{\gamma}\right.$$
$$\left.+\frac{\bar{\gamma}^2+k^2}{3}-\left(\frac{5}{2}+\frac{k^2}{2\bar{\gamma}^2}\right)\sin^2\bar{\gamma}\right]\Big/\left[\frac{\bar{\gamma}^2+k^2}{2}\left(1-\frac{\sin 2\bar{\gamma}}{2\bar{\gamma}}\right)\right]. \tag{C 6}$$

A similar analysis for equation (12) gives

$$\psi_1 = \cos(\gamma_n y) \quad \text{and} \quad \psi_2 = \frac{\sin(\gamma_n y)}{\gamma_n}, \tag{C 7a, b}$$

where

$$\gamma_n = (n+\tfrac{1}{2})\pi \quad (n = 0, 1, 2, \ldots). \tag{C 8}$$

For the Fourier transform of the induced (symmetric) normal vorticity the two parts become

$$\hat{\omega}_{1s} = \mathrm{i}kR\,\mathrm{e}^{-\bar{\sigma}t/R}\frac{A}{2\bar{\gamma}}\left\{\left[1-y^2-\frac{8\bar{\gamma}^2}{(\bar{\gamma}^2+k^2)^2}-\frac{\tan\bar{\gamma}}{\bar{\gamma}}\left(1-\frac{4\bar{\gamma}^2}{\bar{\gamma}^2+k^2}\right)\right]\cos(\bar{\gamma}y)\right.$$
$$\left.+y\frac{\sin(\bar{\gamma}y)}{\bar{\gamma}}-\frac{4\bar{\gamma}\sin\bar{\gamma}}{\bar{\gamma}^2+k^2}y\frac{\sinh(ky)}{\sinh k}+\frac{8k\bar{\gamma}\sin\bar{\gamma}}{(\bar{\gamma}^2+k^2)^2}\frac{\cosh(ky)}{\sinh k}\right\} \tag{C 9a}$$

and

$$\hat{\omega}_{2s} = \mathrm{i}kR(\bar{\gamma}^2+k^2)A\sum_n \mathrm{e}^{-\sigma_n t/R}\cos(\gamma_n y)\frac{4\gamma_n\sin\gamma_n}{(\gamma_n^2+k^2)(\bar{\gamma}^2-\gamma_n^2)^2}$$
$$\times\left[\sin\bar{\gamma}+2\bar{\gamma}\cos\bar{\gamma}\left(\frac{1}{\bar{\gamma}^2-\gamma_n^2}-\frac{1}{\gamma_n^2+k^2}\right)\right]. \tag{C 9b}$$

Since $\hat{\omega}_{1s}+\hat{\omega}_{2s} = 0$ at $t/R = 0$, the term in curly brackets in $\hat{\omega}_{1s}$ can be eliminated and the following expression for $\hat{\omega}_s$ is finally obtained:

$$\hat{\omega}_s = -\mathrm{i}kR(\bar{\gamma}^2+k^2)A\sum_n(\mathrm{e}^{-\bar{\sigma}t/R}-\mathrm{e}^{-\sigma_n t/R})\cos(\gamma_n y)$$
$$\times\frac{4\gamma_n\sin\gamma_n}{(\gamma_n^2+k^2)(\bar{\gamma}^2-\gamma_n^2)^2}\left[\sin\bar{\gamma}+2\bar{\gamma}\cos\bar{\gamma}\left(\frac{1}{\bar{\gamma}^2-\gamma_n^2}-\frac{1}{\gamma_n^2+k^2}\right)\right], \tag{C 9c}$$

where

$$\sigma_n = \gamma_n^2+k^2, \tag{C 10}$$

and

$$\bar{\sigma} = \bar{\gamma}^2+k^2. \tag{C 11}$$

The phase speed for the free vorticity modes becomes

$$c_n = \frac{2}{3} + \frac{1}{2\gamma_n^2}. \tag{C 12}$$

The corresponding result for a symmetric O–S eigenfunction is

$$\bar{\phi}_{0s} = \frac{S}{\cosh k}[\cosh k \cos(\bar{\gamma} y) - \cos\bar{\gamma}\cosh(k\bar{\gamma})] \tag{C 13}$$

where
$$S^2 = \frac{2k^2}{(\bar{\gamma}^2 + k^2)(1 + \sin 2\bar{\gamma}/2\bar{\gamma})}, \tag{C 14}$$

and
$$\bar{\gamma}\tan\bar{\gamma} = -k\tanh k. \tag{C 15}$$

The phase speed becomes

$$c_0 = \left[\left(-\frac{3}{4} + \frac{k^2}{4\bar{\gamma}^2} + \frac{4\bar{\gamma}^2}{\bar{\gamma}^2 + k^2}\right)\left(1 + \frac{\sin(2\bar{\gamma})}{2\bar{\gamma}}\right) - \left(\frac{\tanh k}{k} + \frac{1}{\cosh^2 k}\right)\cos^2\bar{\gamma} + \frac{\bar{\gamma}^2 + k^2}{3} - \left(\frac{5}{2} + \frac{k^2}{2\bar{\gamma}^2}\right)\cos^2\bar{\gamma}\right] \Big/ \left[\frac{\bar{\gamma}^2 + k^2}{2}\left(1 + \frac{\sin 2\bar{\gamma}}{2\bar{\gamma}}\right)\right] \tag{C 16}$$

and the induced normal vorticity is

$$\hat{\omega}_{1a} = \mathrm{i}kR\,\mathrm{e}^{-\bar{\sigma}t/R}\frac{S}{2\bar{\gamma}}\left\{\left[y^2 - 1 + \frac{8\bar{\gamma}^2}{(\bar{\gamma}^2 + k^2)^2} - \frac{1}{\bar{\gamma}\tan\bar{\gamma}}\left(1 - \frac{4\bar{\gamma}^2}{\bar{\gamma}^2 + k^2}\right)\right]\sin(\bar{\gamma} y) + y\frac{\cos(\bar{\gamma} y)}{\bar{\gamma}} - \frac{4\bar{\gamma}\cos\bar{\gamma}}{\bar{\gamma}^2 + k^2}y\frac{\cosh(ky)}{\cosh k} + \frac{8k\bar{\gamma}\cos\bar{\gamma}}{(\bar{\gamma}^2 + k^2)^2}\frac{\sinh(ky)}{\cosh k}\right\} \tag{C 17a}$$

$$\hat{\omega}_{2a} = -\mathrm{i}kR(\bar{\gamma}^2 + k^2) \times S\sum_n \mathrm{e}^{-\sigma_n t/R}\sin(\gamma_n y)\frac{4\gamma_n\cos\gamma_n}{(\gamma_n^2 + k^2)(\bar{\gamma}^2 - \gamma_n^2)^2}\left[\cos\bar{\gamma} - 2\bar{\gamma}\sin\bar{\gamma}\left(\frac{1}{\bar{\gamma}^2 - \gamma_n^2} - \frac{1}{\gamma_n^2 + k^2}\right)\right] \tag{C 17b}$$

which, as in the previous case, can be reduced to

$$\hat{\omega}_a = \mathrm{i}kR(\bar{\gamma}^2 + k^2) \times S\sum_n (\mathrm{e}^{-\bar{\sigma}t/R} - \mathrm{e}^{-\sigma_n t/R})\sin(\gamma_n y)\frac{4\gamma_n\cos\gamma_n}{(\gamma_n^2 + k^2)(\bar{\gamma}^2 - \gamma_n^2)^2}\left[\cos\bar{\gamma} - 2\bar{\gamma}\sin\bar{\gamma}\left(\frac{1}{\bar{\gamma}^2 - \gamma_n^2} - \frac{1}{\gamma_n^2 + k^2}\right)\right] \tag{C 17c}$$

where now
$$\gamma_n = n\pi \quad (n = 1, 2, \ldots). \tag{C 18}$$

Also, the expression (C 10)–(C 12) apply.

The algebra was checked with a commercially available program for symbolic manipulation, MAPLE, developed by Symbolic Computation Group, University of Waterloo, Canada. Also, the results for the energy density were compared to numerically obtained results at $\alpha R = 1$. Even at this value, the asymptotic results for $\alpha R = 0$ differed only marginally from the full numerical solution.

REFERENCES

ALAVYOON, F., HENNINGSON, D. S. & ALFREDSSON, P. H. 1986 Turbulent spots in plane Poiseuille flow–flow visualization. *Phys. Fluids* **29**, 1328–1331.

BENNEY, D. J. & GUSTAVSSON, L. H. 1981 A new mechanism for linear and nonlinear hydrodynamic instability. *Stud. Appl. Maths* **64**, 185–209.

CARLSON, D. R., WIDNALL, S. E. & PEETERS, M. F. 1982 A flow visualization study of transition in plane Poiseuille flow. *J. Fluid Mech.* **121**, 487–505.

CHAMBERS, F. W. & THOMAS, A. S. W. 1983 Turbulent spots, wave packets and growth. *Phys. Fluids* **26**, 1160–1162.

DAVEY, A. & REID, W. H. 1977 On the stability of stratified viscous plane Couette flow. Part 1. Constant buoyancy frequency. *J. Fluid Mech.* **80**, 509–525.

DRAZIN, P. & REID, W. 1981 *Hydrodynamic Stability*. Cambridge University Press.

ELLINGSEN, T. & PALM, E. 1975 Stability of linear flow. *Phys. Fluids* **18**, 487–488.

GUSTAVSSON, L. H. 1981 Resonant growth of three-dimensional disturbances in plane Poiseuille flow. *J. Fluid Mech.* **112**, 253–264.

GUSTAVSSON, L. H. 1986 Excitation of direct resonances in plane Poiseuille flow. *Stud. Appl. Maths* **75**, 227–278.

GUSTAVSSON, L. H. & HULTGREN, L. S. 1980 A resonance mechanism in plane Couette flow. *J. Fluid Mech.* **98**, 149–159.

HENNINGSON, D. S. 1990 An eigenfunction expansion of localized disturbances. *Poster presented at 3rd European Turbulence Conf., Stockholm.*

HENNINGSON, D. S., JOHANSSON, A. V. & LUNDBLADH, A. 1989 On the evolution of localized disturbances in laminar shear flows. *Paper presented at the 3rd IUTAM Symp. on Laminar–Turbulent Transition, Toulouse.*

HERBERT, T. 1983 Stability of plane Poiseuille flow. Theory and experiment. *Fluid Dyn.* **11**, 77–126.

HERBERT, T. 1988 Secondary instability of boundary layers. *Ann. Rev. Fluid Mech.* **20**, 487–526.

HULTGREN, L. S. & GUSTAVSSON, L. H. 1981 Algebraic growth of disturbances in a laminar boundary layer. *Phys. Fluids* **24**, 1000–1004.

KIM, J. & MOSER, R. D. 1989 On the secondary instability in plane Poiseuille flow. *Phys. Fluids* A **1**, 775–777.

KLINGMANN, B. G. B. & ALFREDSSON, P. H. 1990 Experiments on the evolution of a point-like disturbance in plane Poiseuille flow into a turbulent spot. *Paper presented at 3rd European Turbulence Conf., Stockholm.*

LANDAHL, M. T. 1980 A note on an algebraic instability of inviscid parallel shear flows. *J. Fluid Mech.* **98**, 243–251.

LINDBERG, P-Å., FAHLGREN, M. E., ALFREDSSON, P. H. & JOHANSSON, A. V. 1984 An experimental study of the structure and spreading of turbulent spots. In *Proc. 2nd IUTAM Symp. on Laminar–Turbulent Transition* (ed. V. V. Kozlov), pp. 617. Springer.

MORKOVIN, M. V. 1978 Instability, transition to turbulence and predictability. *AGARDograph No.* 236.

SHANTHINI, R. 1989 Degeneracies of the temporal Orr–Sommerfeld eigenmodes in plane Poiseuille flow. *J. Fluid Mech.* **201**, 13–34.

WYGNANSKI, I., HARITONIDIS, J. & KAPLAN, R. E. 1979 On a Tollmien–Schlichting wave packet produced by a turbulent spot. *J. Fluid Mech.* **92**, 505–528.